ORIGINAL PAPER

Scalable Generation of Hybrid Graphene Nanoscrolls for High-Performance Solid Lubricants

Pratik S. Kasbe[1] · Juan Bosch[2] · Jinyu Bu[1] · Christopher DellaCorte[2] · Weinan Xu[1]

Abstract

Graphene and other 2D materials have been extensively studied as solid lubricants in recent years. Low friction can sometimes be observed in those 2D lubricants, and one possible mechanism is that scroll-shaped nanostructures are formed during friction, which decreases the contact area and energy barrier, thus substantially reducing friction. The integration of graphene with metal or metal oxide nanostructures can further enhance its lubrication properties by increasing film formation ability and easy shearing of the nanosheets. However, it is not possible to reliably promote the formation of such nanoscroll-shaped low friction wear products, which limits the reproducibility and application of such nanostructures as solid lubricants. In this study, we address this issue by creating a scalable method for the synthesis of hybrid graphene-titanium oxide (G–TiO$_2$) nanoscrolls and demonstrating their potential as solid lubricants with macroscopic coefficient of friction as low as 0.02 in ambient conditions. Our approach to generate the nanoscrolls is based on the in situ sol–gel synthesis of TiO$_2$ on graphene followed by spray-freeze-drying–induced shape transformation. The solid lubrication performance of such G–TiO$_2$ nanoscrolls can be further enhanced by applying a thin graphene oxide primer layer, which provides high affinity to both the substrate and the active materials. These hybrid nanoscrolls hold promising potential for applications in aerospace, automotive, and precision manufacturing fields as effective solid lubricants.

Graphical Abstract
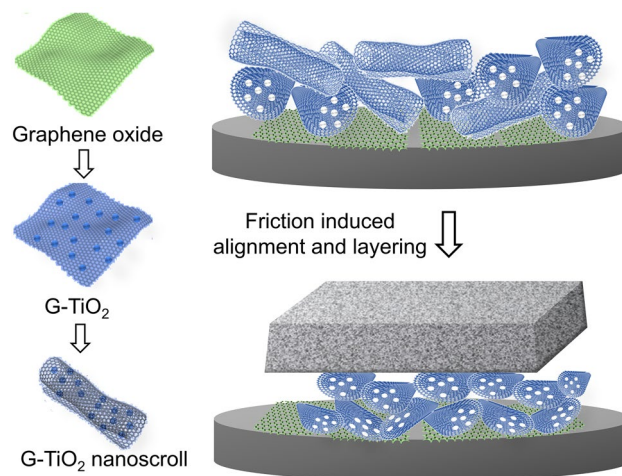
Extended author information available on the last page of the article

1 Introduction

Solid lubricants are widely used in many applications involving harsh environments such as aerospace, automotive, and nuclear energy [1, 2].] They are critical to the improvement of energy efficiency of moving mechanical systems and the reduction of carbon footprint [3, 4]. Graphite and molybdenum disulfide (MoS_2) are among the most commonly used solid lubricants [5, 6]. They are usually applied as thin films by physical vapor deposition (PVD) and/or chemical vapor deposition (CVD) [7]. Such "bulk" thin films typically provide friction coefficients of around 0.1 in pure sliding owing to their easy shear properties. Being thin films of finite thickness, wear life is limited, and replenishment is a challenge [8].

In recent years, atomically thin 2D materials, especially graphene, graphene oxide (GO), and 2D MoS_2, have been extensively studied to overcome certain limitations of their bulk counterparts because those nanosheets can be easily applied and replenished [9–12]. However, the main drawbacks of atomically thin 2D materials as solid lubricants include easy aggregation, limited stability, and inconsistent performance at the macroscale [13, 14].

Several previous studies have found that during the friction process of graphene or other carbon-based solid lubricants (amorphous carbon and diamond-like carbon), graphene nanoscrolls can be formed. Nanoscrolls are thin layers of material that roll-up upon themselves to form a scroll-like structure. Such nanoscrolls are critical to reducing contact area and coefficient of friction [15, 16]. For instance, Berman et al. showed that superlubricity, defined as coefficient of friction (COF) less than 0.01, can be realized at engineering scale in a nitrogen environment when graphene was used in combination with nanodiamond particles and diamond-like carbon [15]. The graphene sheets wrapped around nanodiamonds to form nanoscrolls at the sliding interface. Graphene nanoscrolls (NS) consisting of graphene shell and amorphous carbon core have also been observed in tribofilm formed by amorphous carbon coating [16], which is believed to be the main reason for achieving low friction. In another report, macroscale superlubricity at ambient conditions was achieved when graphene-coating microspheres were used as solid lubricants between the graphene-coated plate and ball [17].

Despite the importance and high potential of graphene nanoscrolls in achieving macroscopic superlubricity, it is very challenging to generate them in a controlled or scalable way. In the above-mentioned studies, graphene nanoscrolls are formed among the wear products during the friction process, which is not efficient or well controlled. There are a few recent reports on bottom-up approach for the synthesis of graphene nanoscrolls [18–21], but such nanoscrolls have quite different structures and sizes, and they have yet to be investigated for solid lubrication applications.

Moreover, it is important and beneficial to integrate inorganic nanoparticles (NPs) within the graphene to further enhance their solid lubrication performance [22, 23]. The metal or metal oxide nanoparticles provide robust film formation ability or act as nano-scale ball bearings in addition to the easy shearing of graphene nanosheets, which usually leads to enhanced lubrication especially under harsh conditions [24–26]. The inorganic nanoparticles that have been combined with graphene for lubrication applications include Cu, Ag, Al_2O_3, Fe_3O_4, Mn_3O_4, etc. [11, 27]. It is relatively simple to incorporate 2D graphene nanosheets with inorganic NPs by direct mixing or bottom-up synthesis. But it is more challenging to incorporate graphene nanoscrolls with inorganic NPs due to the 1D morphology and size mismatch. To the best of our knowledge, such hybrid graphene nanoscrolls from bottom-up synthesis have never been explored for lubrication applications.

To address those issues and fill the knowledge gap, here we report a scalable method for the synthesis of hybrid graphene-titanium oxide (G–TiO_2) nanoscrolls and study their potential as solid lubricants. Our method for creating the hybrid nanoscrolls is based on in situ sol–gel synthesis of TiO_2 on graphene followed by spray-freeze-drying-induced shape transformation. Such G–TiO_2 nanoscrolls show macroscopic coefficient of friction of around 0.1 at ambient conditions, which can be further improved to as low as 0.02 when graphene oxide is used as the primer layer. The high solid lubrication performance can be related to the unique sharkskin-like morphology formed by the alignment and assembly of those hybrid nanoscrolls during friction.

2 Materials and Methods

2.1 Materials

Graphite powder, potassium permanganate, sodium bicarbonate, tris–HCl buffer, ammonium hydroxide solution (28–30%), titanium (IV) n-butoxide, and ethanol were all purchased from Sigma-Aldrich and used as received. Sulfuric acid and hydrogen peroxide were purchased from VWR Chemicals and used as received. Hydrazine monohydrate (98%) was purchased from Fisher Scientific. Silicon wafers with a diameter of 2 inch were purchased from UniversityWafer.

2.2 *Preparation of G–TiO$_2$ nanoscrolls*

Graphene oxide (GO) nanosheets were prepared by a modified Hummer's method as described in our previous

report [28]. For the in situ sol–gel synthesis of TiO_2 on GO nanosheets, the GO water suspension (0.1 mg/mL, 200 mL) was first solvent exchanged with ethanol to get GO ethanol suspension. Then, 0.4 mL of ammonium hydroxide was added to the solution and stirred for 30 min at 25 °C. Titanium (IV) n-butoxide (3 mL or 1.5 mL) was then added dropwise to the solution and kept for stirring at 25 °C for 24 h. After the sol–gel reaction, the product was washed by centrifugation and replaced the supernatant with DI water, and the washing was repeated three times.

The GO-TiO_2 nanosheets prepared from the previous step were dispersed in DI water and added to a glass flask. A mixture of 40-μl hydrazine monohydrate and 280-μl ammonium hydroxide was slowly added to the flask while stirring. The flask was then put in an oil bath heated to 95 °C and kept for 1 h. During this step, the reduction of GO to graphene as well as the amorphous to crystalline transition of TiO_2 nanostructures took place, and the product is named G-TiO_2 nanosheets.

The G-TiO_2 nanosheets water suspension was then directly sprayed into a container filled with liquid nitrogen using a spray gun. The frozen sample was then freeze-dried at -58 °C to obtain the final product, which is G–TiO_2 NS.

2.3 Tribology Characterization

A controlled amount of G–TiO_2 NS was dispersed in ethanol to prepare a uniform suspension (0.5 mg/mL). The suspension (20 mL) was then drop casted on a 2-inch silicon wafer and after evaporation of ethanol, a uniform coating layer was formed on the wafer. Other control samples were prepared in the same way by drop casting on silicon wafer from their corresponding ethanol suspensions. For coatings with graphene or GO primer layer, graphene or GO ethanol suspension was used to drop cast and obtain the primer layer, followed by drop casting of the G–TiO_2 NS.

The coefficient of friction (COF) was measured using CSEM High-Temperature Pin-on-disk tribometer. Stainless Steel (SS) balls (440 C) with a diameter of 6 mm were used. The substrates are silicon wafers with different coatings mentioned above. The normal load was varied in the range of 2 N to 5 N with a maximum Hertz contact pressures of 0.74 and 1 GPa, respectively. The linear speed of the ball was kept at 5 cm/s for a total sliding distance ranging from 50 to 100 m. The data collection frequency was 7 Hz. All the measurements were conducted in ambient conditions with temperature around 25 °C and humidity around 50%.

2.4 Other Characterization

Scanning electron microscopy (SEM) was conducted using JEOL-7401 FE-SEM at an accelerating voltage of 10 kV. Transmission electron microscopy (TEM) images were obtained using Tecnai G2 F20 at an acceleration voltage of 110 kV. Raman spectra were collected with a Renishaw inVia confocal Raman microscope with an excitation laser of wavelength 514 nm. Optical profilometer (Zygo NewView 7300) was used for studying the dimension and morphology of the wear tracks and balls. Olympus BX51 optical microscope was used for capturing optical images. X-ray photoelectron spectroscopy (XPS) was conducted with a PHI VersaProbe III surface analysis instrument (Physical Electronics) at a 45° take-off angle. Surveys were conducted at a pass energy of 117 eV and high-resolution spectra were obtained at a pass energy of 11.7 eV.
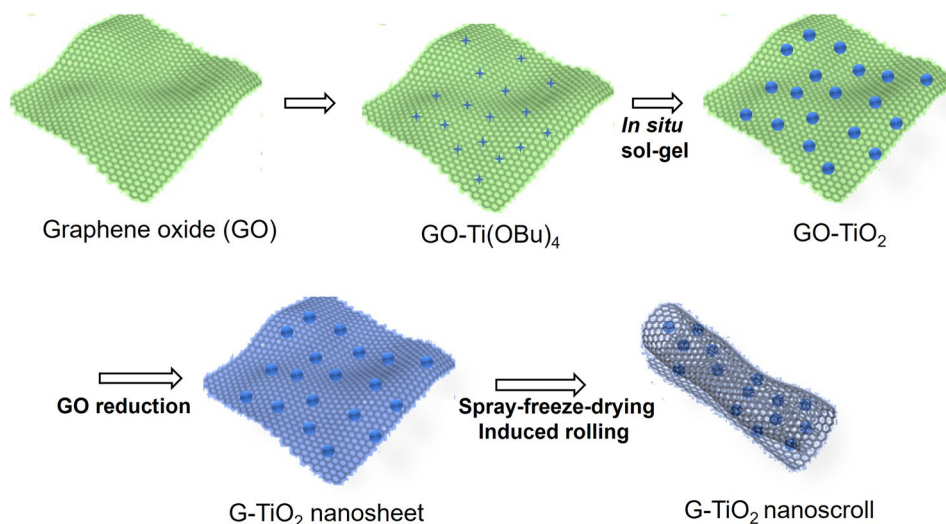
3 Results and Discussion

3.1 *Synthesis and Characterization of the G–TiO_2 Nanoscrolls*

The fabrication process of the G–TiO_2 hybrid nanoscrolls is shown in Fig. 1. Briefly, in situ sol–gel synthesis of TiO_2 was conducted on the GO surface in ethanol using titanium butoxide as the precursor. During this step, the hydrolysis and subsequent polycondensation reaction occur to form amorphous TiO_2 network. Subsequently, the hybrid nanosheets were chemically reduced by a hydrazine/ammonia mixture. During this step, GO was reduced to reduced graphene oxide, which is referred to as graphene here for simplicity, although the structure is different from physically exfoliated graphene. Meanwhile, the hydrazine acted as a catalyst to further promote the dehydroxylation and polycondensation reaction of amorphous TiO_2 on graphene surface [29]. In addition, the heating (95 °C) during the hydrazine reduction step promotes the transition of amorphous TiO_2 to crystalline structures, as confirmed by spectroscopy data in the following discussion.

The as-prepared G–TiO_2 hybrid nanosheets were transformed into nanoscrolls through a scalable spray-freeze-drying method. This method has been used to prepare simple graphene nanoscrolls [18, 19]. In our case, the prepared G–TiO_2 hybrid nanosheets were dispersed in DI water, and the dispersion was sprayed directly into liquid nitrogen to achieve very fast freezing. Then, the frozen sample was freeze-dried, and during the sublimation process of ice, the 2D nanosheets transformed into nanoscrolls. Such shape transformation process was induced by the competition between the elastic bending energy and free energy. When the scrolling occurs, there is a decrease in the surface free energy of the hydrophobic graphene nanosheets originating from the van der Waals interaction of the overlapping domains; at the same time, there is an increase in the elastic energy caused by rolling and distorting of the graphene. When the former overweighs the latter, spontaneous

Fig. 1 Schematic of the in situ sol–gel synthesis and shape transformation to generate the G-TiO$_2$ NS

Graphene oxide (GO) GO-Ti(OBu)$_4$ *In situ sol-gel* GO-TiO$_2$

GO reduction G-TiO$_2$ nanosheet Spray-freeze-drying Induced rolling G-TiO$_2$ nanoscroll

formation and stabilization of G–TiO$_2$ NS takes place, as is the case for our system.

The morphology of the fabricated G–TiO$_2$ NS as well as graphene NS (as a control sample) was studied with SEM and TEM. A dense network of the formed graphene NS can be seen in SEM image (Fig. 2a), the average length is on the order of one to several µm, and the average diameter is on the order of 10 nm. TEM image of the graphene NS (Fig. 2b) further confirms the tubular shape of the NS with multilayered graphene shell. When TiO$_2$ is integrated by in situ sol–gel synthesis, the formed G–TiO$_2$ NS maintains the nanoscroll shape (Fig. 2c), while the average diameter is increased to about 50 nm, and the hybrid NS have higher degree of curling compared with pristine graphene NS. High-resolution TEM image (Fig. 2d) further shows that TiO$_2$ nanostructures exist on both the surface and interior of the G-TiO$_2$ NS. In addition, we studied another control sample: the physical mixture of graphene and TiO$_2$ NPs by

SEM (fig S1), which does not show such rolled-up morphology, and the two components are randomly distributed or aggregated in the mixture.

Raman spectroscopy was used to characterize the structure of the G–TiO$_2$ NS as well as its precursors and control samples (Fig. 3a). Graphene shows its characteristic G band at 1596 cm^{-1}, D band at 1348 cm^{-1}, 2D bands at 2677 cm^{-1}, as well as the D + G band at 2865 cm^{-1} [30]. As a control sample, the TiO$_2$ NPs prepared by hydrothermal method show Raman peaks at 145, 394, 515, and 637 cm^{-1}, which indicates the TiO$_2$ NPs have anatase crystalline structure. Raman spectrum of the physical mixture of graphene and TiO$_2$ NPs (Figure S2) shows the characteristic graphene G, D, and 2D bands, as well as the anatase TiO$_2$ peaks at 145, 394, and 630 cm^{-1}.

Raman spectrum of the G–TiO$_2$ NS shows the D and G bands of graphene, but interestingly, the peaks for TiO$_2$ component are located at 150, 257, 421, and 610 cm^{-1}, which

Fig. 2 Morphological study of graphene and G-TiO$_2$ nanoscrolls. **a** SEM of graphene nanoscrolls, **b** TEM of one representative graphene nanoscroll, **c** SEM of G-TiO$_2$ nanoscrolls, and **d** TEM of one representative G-TiO$_2$ nanoscroll
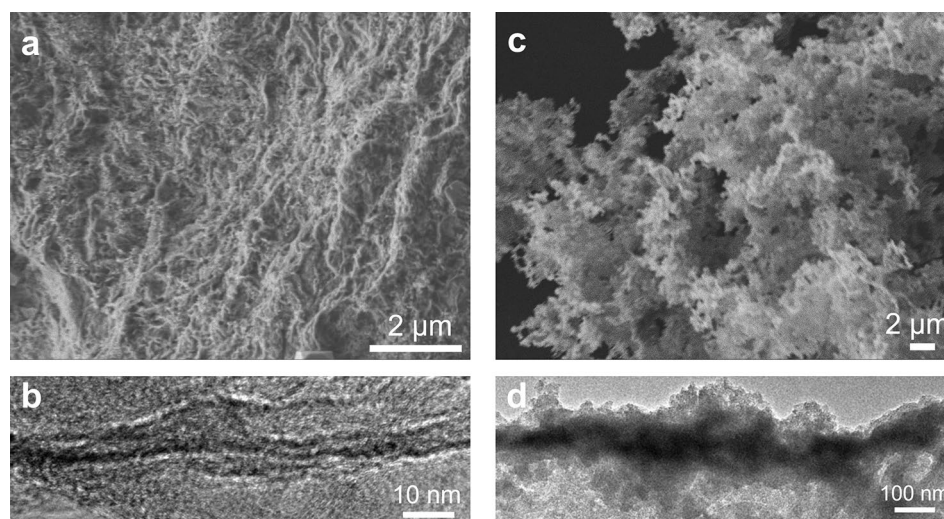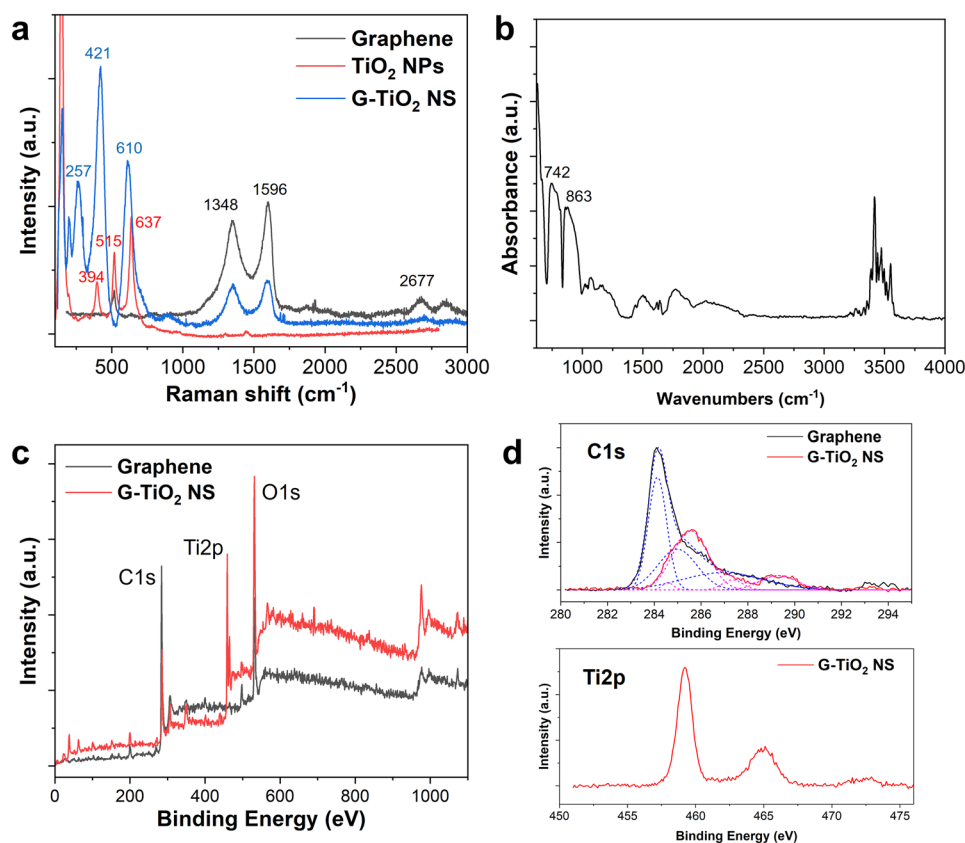
Fig. 3 Spectroscopy characterization of the G-TiO$_2$ NS and control samples. **a** Raman spectra of the G–TiO$_2$ NS and control samples: graphene and TiO$_2$ NPs. **b** FTIR spectrum of the G–TiO$_2$ NS. **c** XPS spectra of graphene and G-TiO$_2$ NS. **d** High-resolution XPS scan of the C1s and Ti2p peaks for graphene and/or G–TiO$_2$ NS

indicate the TiO$_2$ nanostructures in the G–TiO$_2$ NS have primarily rutile crystalline phase [31], which are different from the control TiO$_2$ NPs prepared by hydrothermal method. The crystalline structure of TiO$_2$ in the G–TiO$_2$ NS will also undergo interesting transformation during the friction process, as will be discussed later.

FTIR was used to characterize the chemical structure of the G–TiO$_2$ NS (Fig. 3b). The peak at 742 cm^{-1} corresponds to Ti–O–Ti bond [32], and the peak at 863 cm^{-1} corresponds to Ti–O–C bond [33]. Such results indicate that there are chemical interactions and bond formation between graphene and TiO$_2$ in the G–TiO$_2$ NS. The peaks at around 1600 cm^{-1} and 3500 cm^{-1} are ascribed to bending vibration and stretching vibration of H–O–H and O–H, which comes from the absorption of moisture on the surface of G–TiO$_2$ NS.

X-ray photoelectron spectroscopy (XPS) provides further information on the structure and composition of the samples (Fig. 3c). The survey XPS scan shows that graphene has a pronounced C1s peak as well as an O1s peak. The O1s peak mainly originates from the underlying SiO$_2$ substrate as well as a small amount of residual C–O groups on graphene. The G–TiO$_2$ NS, on the other hand, has not only C1s and O1s peaks but also a substantial Ti2p peak due to the in situ-synthesized TiO$_2$ nanostructures.

High-resolution XPS scans of the C1s peaks and peak fittings are shown in Fig. 3d. The C1s peak of graphene can

be deconvoluted into a strong sp2 carbon peak at 284.1 eV, sp3 carbon peak at 285.0 eV, as well as a small C–O peak at 287.1 eV. For G–TiO$_2$ NS, the C1s peak not only has contribution from the above-mentioned three components, but also an additional peak at 289.3 eV, which can be ascribed to the Ti–O–C=O structure [34].

High-resolution scan of Ti2p peak for G–TiO$_2$ NS is shown in Fig. 3e. The Ti2p3/2 and Ti2p1/2 peaks appear at 459.2 eV and 465.0 eV, respectively. Moreover, the highly symmetric Ti2p3/2 peak indicates the absence of other types of titanium sub-oxides [35]. High-resolution scan of O1s peak and fitting (Figure S3) shows that graphene has a peak at 532.0 eV from the underlying SiO$_2$ substrate. G–TiO$_2$ NS has two deconvoluted peaks at 532.0 and 530.8 eV, the former is ascribed to SiO$_2$ substrate, and the latter is ascribed to Ti–O lattice.

3.2 Tribological Properties as Solid Lubricants

Both graphene and TiO$_2$ nanostructures have shown great potential to be used as high-performance solid lubricants, thus it is hypothesized that the synergy of graphene and TiO$_2$ in the G–TiO$_2$ NS would lead to further enhancement in solid lubrication properties (Fig. 4). The reduced contact area as well as the rolling of G-TiO$_2$ NS during friction are expected to substantially reduce the COF.

Fig. 4 Schematic of the pin-on-disk tribology study with the G–TiO$_2$ NS as the solid lubricant and an optional primer layer
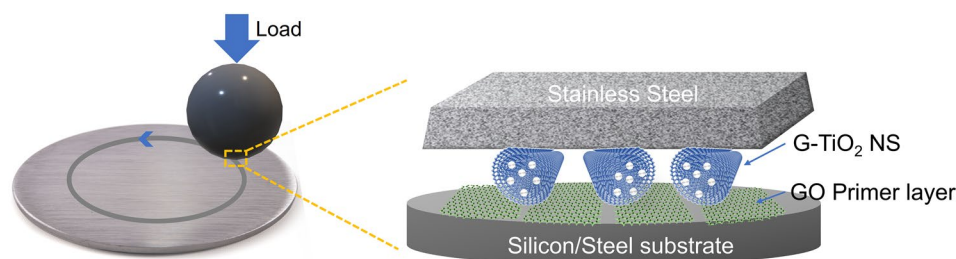
To have a systematic investigation and understanding of the G–TiO$_2$ NS lubrication properties, we first studied several important control samples. Firstly, graphene and graphene oxide coatings on silicon substrates were studied with a pin-on-disk tribometer (Fig. 5a). The normal load was 2 N, and the linear speed was 5 cm/s for the testing. Graphene coating shows an average macroscopic COF of 0.22 in ambient environment, which is consistent with previous studies [36]. Graphene oxide has a higher COF of 0.30 in ambient conditions. The main reason for the relatively high COF of GO can be ascribed to the relatively high wear volume and generation of wear particles, as will be discussed in a later section. In addition, due to the presence of abundant functional groups (such as epoxy, hydroxyl, and carboxylic acid), the electrostatic and hydrogen bonding interactions between the graphene oxide layers can also increase the friction and energy barrier between two sliding graphene oxide layers [37].

The solid lubrication property of another control sample: TiO$_2$ NPs, which were prepared by hydrothermal method was also investigated. The results show that under 2-N load and 5-cm/s linear sliding speed, an average COF of 0.24 is observed for TiO$_2$ NPs (Fig. 5b), which is consistent with previous reports [38]. Another important control sample for the G–TiO$_2$ NS is a physical mixture of graphene and TiO$_2$ NPs (with weight ratio of 1.2 to 1). The two components in the physical mixture only have weak physical interaction in contrast to the strong binding in G–TiO$_2$ NS. The average COF for the physical mixture was about 0.3 at the early stage but fluctuated and increased to 0.8 at a longer time. Such behavior can be related to their structure and morphology (figure S1): the physical mixture has loosely connected or aggregated graphene and TiO$_2$ NPs, which leads to poor coating stability and weak adhesion to the Si substrate.

Tribological study of those control samples is important to gain insight into the lubrication properties of G–TiO$_2$ NS. The thickness of such G–TiO$_2$ NS coating on silicon

Fig. 5 Tribological study of the G–TiO$_2$ NS and control samples under ambient conditions, with a load of 2 N and linear sliding speed of 5 cm/s. **a** COF over time of graphene and GO coatings. **b** COF over time of TiO$_2$ NPs and the physical mixture of graphene and TiO$_2$. **c** COF over time of G-TiO$_2$ NS with two different ratios (h: high, l: low) between TiO$_2$ and graphene. **d** COF over time of G-TiO$_2$ NS coating with graphene or GO primer layer
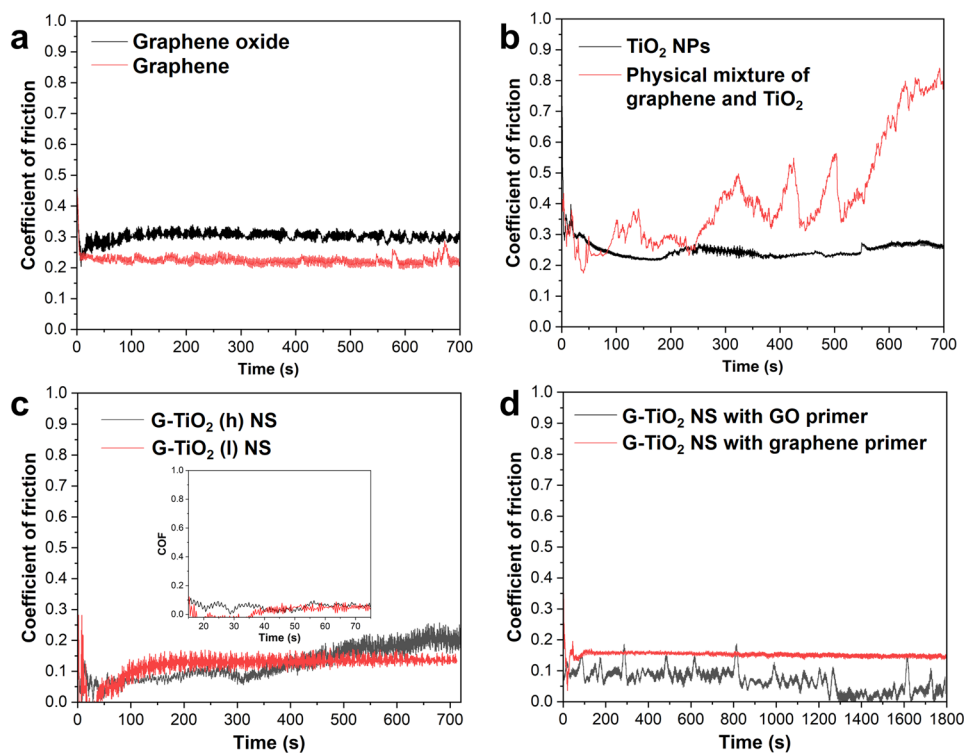
substrate was measured to be around 10.0 μm (Figure S4). Importantly, for the G–TiO$_2$ NS, the ratio between TiO$_2$ and graphene can be varied by adjusting the amount of titanium precursor in the in situ sol–gel synthesis. In our study, two G–TiO$_2$ NS samples with different ratios between the two components were prepared. The first sample has a higher titanium butoxide concentration of 0.044 mol/L and is named G–TiO$_2$ (h) NS in Fig. 5c; the second sample has a lower titanium butoxide concentration of 0.022 mol/L and is named G–TiO$_2$ (l) NS.

The tribological results from pin-on-disk tribology testing (load of 2 N, linear speed of 5 cm/s) of the G-TiO$_2$ NS are shown in Fig. 5c. The steady-state friction coefficients are obtained after a short running-in period. The G–TiO$_2$ (l) NS shows a stable COF of 0.13, a substantial improvement compared with its individual components (graphene or TiO$_2$ NPs). For the G–TiO$_2$ (h) NS with a higher TiO$_2$ content, the COF at the early stage further decreased to 0.07 but increased to 0.17 at longer time (after 500 s). Those results show that the integration of TiO$_2$ and graphene into G–TiO$_2$ NS has a synergistic effect of enhancing the solid lubrication performance compared with the individual components. Such enhancement is mainly due to the unique hybrid nanoscroll structure which creates sliding interface and incommensurate contact area. From this point forward, G–TiO$_2$ NS will be used to denote the G–TiO$_2$ (h) NS unless otherwise specified, based on the better solid lubrication performance of G–TiO$_2$ NS with a higher TiO$_2$ content.

Despite the enhanced lubrication performance, the coating stability of such hybrid nanoscrolls, especially those with high TiO$_2$ to graphene ratio needs to be further improved to maintain the low COF at long running time. To address this issue, we developed a modified procedure using graphene or GO as the primer layer for the hybrid G-TiO$_2$ NS coating. The hypothesis is that the atomically thin graphene or GO nanosheets provide better adhesion to the silicon substrate and improve the overall stability of the coatings. The thickness of such G-TiO$_2$ NS coating with GO primer layer was measured to be around 15.0 μm (Figure S4).

The COF results (under a load of 2 N and linear sliding speed of 5 cm/s) of such coatings with primer layer are shown in Fig. 5d. When graphene is used as the primer layer, the average COF for the G–TiO$_2$ NS is 0.15, which is close or slightly higher than that of G-TiO$_2$ hybrid NS without primer layer. The probable reason is that hydrophobic graphene is not able to form a homogenous primer layer on the hydrophilic silicon wafer. On the other hand, hydrophilic GO can form a uniform primer layer to enhance the adhesion and stability of the NS coating. As a result, the COF for the G-TiO$_2$ NS with GO primer layer is about 0.10 at early stage and then further decreased to 0.02 at longer time (after 1300 s).

3.3 Wear Track and Ball Wear Analysis

To obtain a more systematic understanding of the tribological properties, we analyzed the wear tracks of the samples after pin-on-disk testing with an optical microscope and a white light profilometer (Fig. 6). It can be seen that GO coating has relatively high wear volume, the width of the wear track is about 0.5 mm, and the depth is about 10 μm (Fig. 6 a-c). For the graphene coating, the width of the wear track is about 0.35 mm, and the depth is about 6 μm (Fig. 6d-f). Also, there is a relatively flat film formed in the wear tracks. This result shows that graphene has better wear resistance than GO, which is consistent with previous studies. The probable reason is the larger interlayer distance of GO caused by the presence of functional groups as well as the weaker van der Waals force between neighboring layers, thus compromising the mechanical properties of the coating. The wear track for another control sample: TiO$_2$ NP coating, has a width of 0.32 mm and a depth of 6 μm (Figure S5), which is close to that of graphene coating.

For the G-TiO$_2$ NS coating, the wear track width is about 0.5 mm, and the depth is about 8.5 μm (Fig. 6 g-i). This shows that G–TiO$_2$ NS does not have very good wear resistance by itself. This observation aligns with the tribology data, which illustrates an upward trend in the COF for G–TiO$_2$ NS over longer durations and can be attributed to the increased wear of the coating. When GO is applied as the primer layer for G-TiO$_2$ NS, the wear resistance is significantly improved (Fig. 6j-i. The width of the wear track decreases to about 0.25 mm, and the depth decreases to about 4 μm.

The ball wear rate is another important parameter to evaluate tribological properties. We used optical microscope and profilometer to study the morphology of the ball wear and calculated the ball wear rate (details of the calculation are in the SI). For the control sample, which is a physical mixture of graphene and TiO$_2$, the ball wear is substantial with a wear scar diameter of 0.38 mm and a relatively high wear rate of 1.71×10^{-6} mm^3/N·m (at a load of 2 N and distance of 50 m). For the G-TiO$_2$ NS coating, the wear scar diameter decreases to 0.30 mm, and the wear rate decreases to 6.62×10^{-7} mm^3/N·m (at a load of 2 N and distance of 50 m).

Importantly, when GO was used as the primer layer for the G-TiO$_2$ NS coating, significantly decreased ball wear was observed. For a load of 2 N and sliding distance of 50 m, no noticeable ball wear can be observed (Figure S6). When the load further increases to 5 N, and the sliding distance increases to 100 m, a relatively small wear scar with diameter of 0.15 mm can be observed (Fig. 7e-f) and the calculated wear rate decreases to 8.28×10^{-9} mm^3/N·m, which is two orders of magnitude lower than that of control sample: the physical mixture.
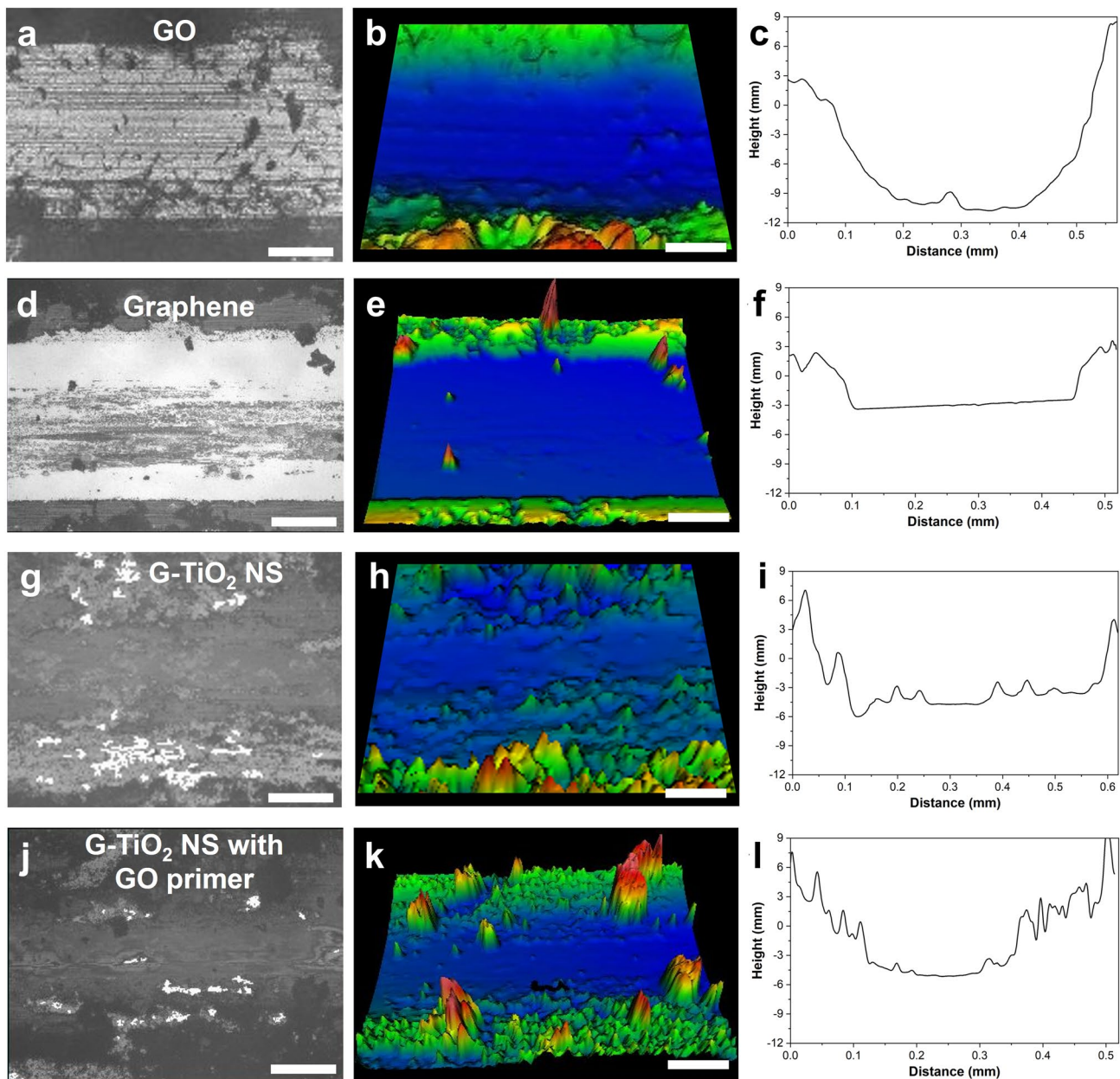
Fig. 6 Wear track characterization of the tribology samples. **a–c** Optical image (**a**), corresponding 3D optical profile (**b**), and cross-section height profile (**c**) of GO coating. **d–f** Optical image (**d**), corresponding 3D optical profile (**e**), and cross-section height profile (**f**) of graphene coating. **g–i** Optical image (**g**), 3D optical profile (**h**), and cross-section height profile (**i**) of G-TiO$_2$ NS coating. **j–l** Optical image (**j**), 3D optical profile (**k**), and cross-section height profile (**l**) of G-TiO$_2$ NS coating with GO primer layer. All scale bars are 100 μm

3.4 Structural Characterization of Wear Tracks

To gain a deeper understanding of the observed tribological properties, we characterized the detailed morphology of the wear tracks formed by the different coatings with SEM. GO can form a uniform coating on the surface of silicon substrate with characteristic wrinkles formed by the atomically thin nanosheets (Fig. 8a). After the pin-on-disk tribology testing, a quite different morphology was observed.

The residual GO forms a flat and compact film with some microcracks formed due to the friction force. Such morphology can be related to the tribological performance of GO coating: the COF is relatively high but very stable due to its strong adhesion to the silicon substrate and the compact structure.

SEM images of the G-TiO$_2$ NS wear track (Fig. 8c-d) show that the NS transformed into a hierarchical structure after tribology testing. The wear track is composed of

Fig. 7 **a–b** Optical microscope image of the ball wear and the corresponding 3D optical profile image of the ball tested on the physical mixture of graphene and TiO_2 NPs. The red arrow indicates the sliding direction. **C–d** Optical microscope image of the ball wear and the corresponding 3D optical profile image of the ball tested on G–TiO_2 NS coating. **e–f** Optical microscope image of the ball wear and the corresponding 3D optical profile image of the ball tested on G–TiO_2 NS with GO primer layer. All scale bars are 100 μm
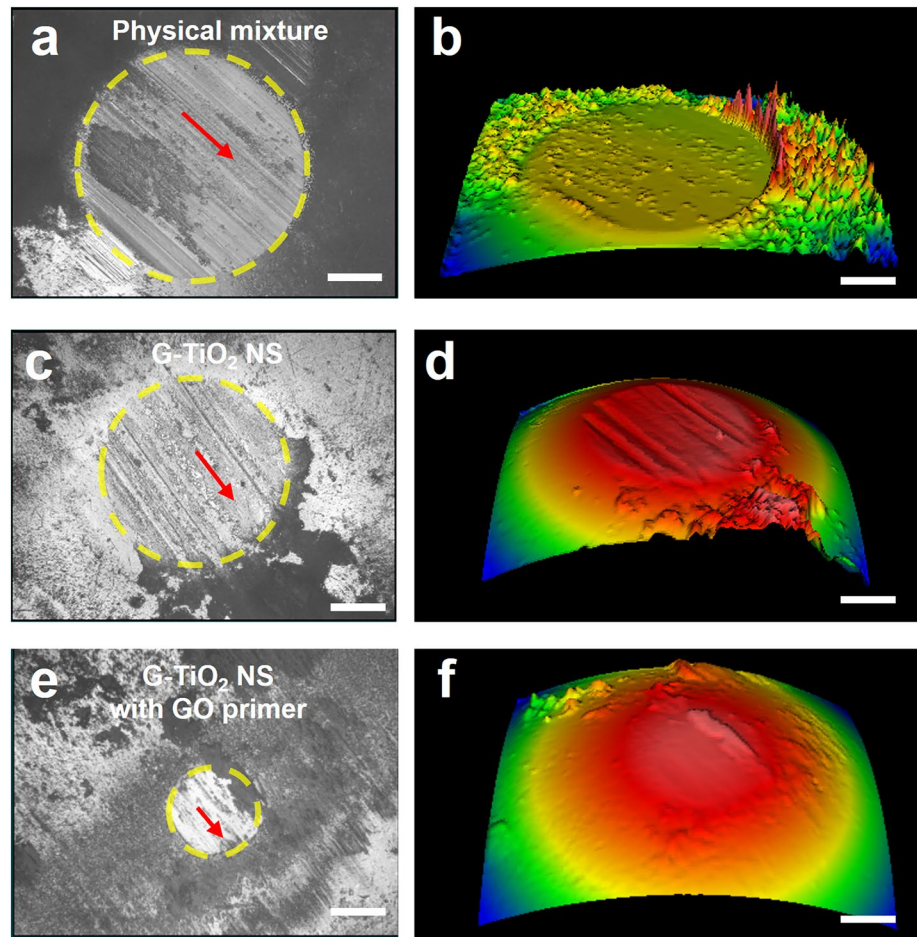
partially overlapping domains similar to that of sharkskin. Wear debris and small voids can also be observed in some locations. For the G–TiO_2 NS with GO as the primer layer, more pronounced sharkskin-like structures can be observed (Fig. 8e-f). There are high density of partially overlapping "scales" in the wear track. The coverage, density, and thickness of those scales are substantially higher than that of the G-TiO_2 NS wear track without GO primer layer. We conducted TEM study of the wear particles from G-TiO_2 NS coating after tribology study (Fig. 8g-h). It can be seen that the G-TiO_2 NS somewhat maintain the scroll-like morphology with TiO_2 nanostructures dispersed in rolled-up graphene, although the nanoscrolls are less well defined and have more interconnected structure compared with those before tribology testing.

We also characterized the wear tracks with Raman spectroscopy (Figure S7). For graphene coating after tribology testing, there are only very weak peaks corresponding to the G and D band of graphene that can be observed. For TiO_2 NPs coating after testing, there is no visible peak except for the underlying Si substrate, which indicates complete removal of the coating. For the physical mixture of graphene and TiO_2 NPs, only the G and D bands of graphene at

1596 and 1348 cm^{-1} were observed, which shows that TiO_2 NPs were mostly lost due to the weak physical interaction between graphene and TiO_2 NPs. On the other hand, for the G-TiO_2 NS wear tracks, besides the G, D, and 2D bands for graphene, interestingly, peaks for anatase TiO_2 at 394, 515, and 637 cm^{-1} were also observed. This result shows that there is a rutile to anatase transformation of the TiO_2 nanostructures in G-TiO_2 NS during mechanical friction, which has not been observed before.

The possible mechanism for the formation of such hierarchical sharkskin-like morphology is shown in Fig. 8i. The as-deposited G-TiO_2 NS has a random orientation and distribution in the coating layer. During the tribology test, the application of normal force and the lateral friction force can effectively induce the rolling and alignment of the G-TiO_2 NS. Many of the NS also undergoes deformation or become partially collapsed during the friction process. Multilayered structures with each layer consisting of closely packed NS can be formed in the wear track, which mimics the structure of sharkskin. Such sharkskin-like morphology decreases the contact area and reduces the shear stress during the friction process [39, 40], which contributes to the substantially enhanced solid lubrication performance of the G-TiO_2 NS.
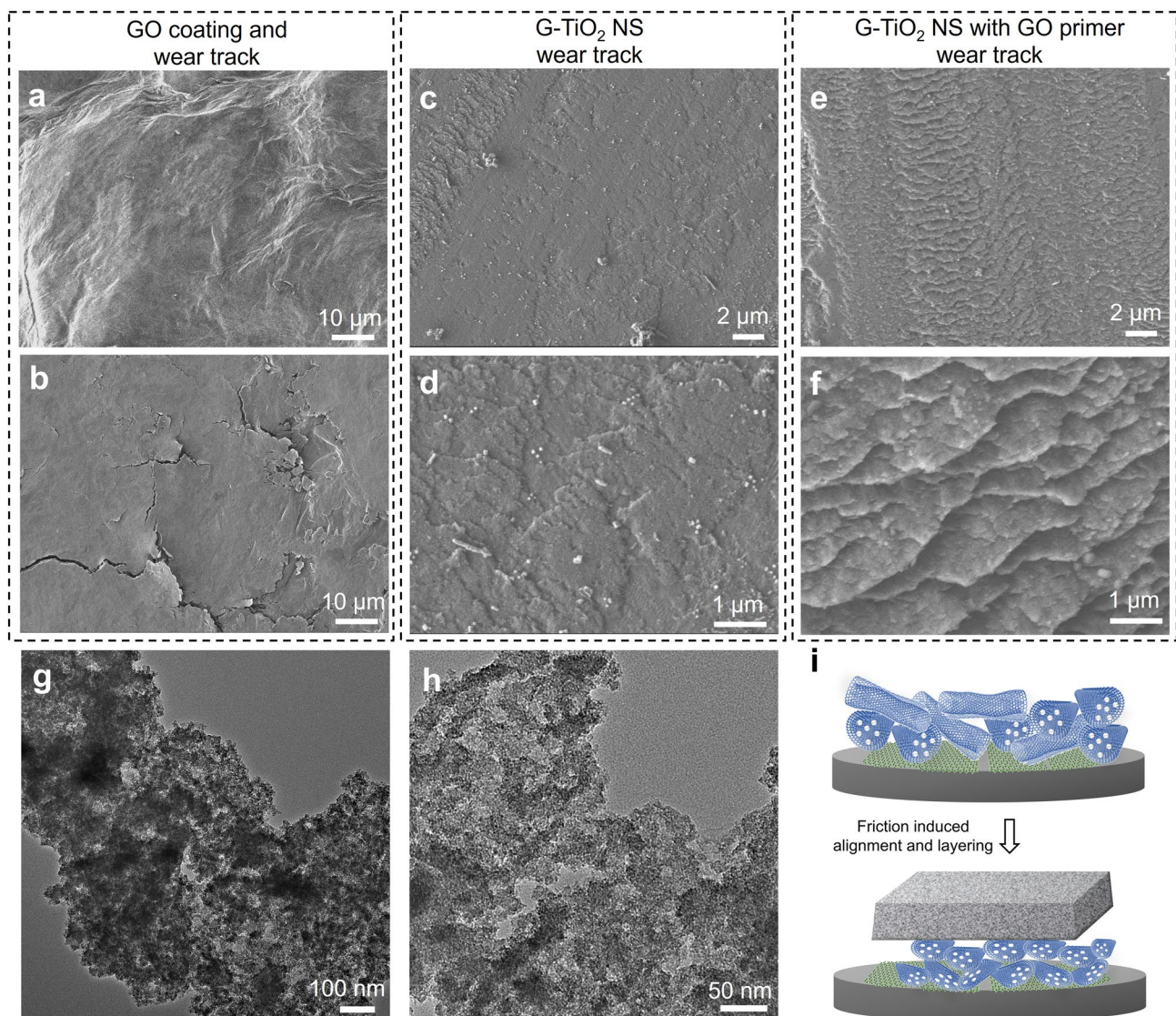
Fig. 8 a SEM image of the pristine GO coating. **b** SEM image of the GO coating wear track. **C–d** SEM image of the wear track from G–TiO$_2$ NS coating at different magnifications. (**e–f**) SEM image of the wear track from G–TiO$_2$ NS coating with GO primer layer at differ-ent magnifications. (**g–h**) TEM images of the wear particles from G–TiO$_2$ NS coating after tribology study at two different magnifications. **i** Schematic representation of the possible mechanism for the friction-induced alignment and layering of G–TiO$_2$ NS

4 Conclusion

An efficient and scalable method for the controlled synthesis of hybrid graphene nanoscrolls was developed. This method integrates in situ sol–gel metal oxide synthesis and spray-freeze-drying-induced shape transformation of graphene. The generated G–TiO$_2$ NS have well-defined size, shape, and tunable composition. The COF of such G–TiO$_2$ NS measured under ambient conditions is around 0.10, which is substantially lower than its individual components: graphene or TiO$_2$ NPs, also much lower than the physical mixture of graphene and TiO$_2$ NPs. Moreover, with the application of GO as the primer layer for such G–TiO$_2$ NS coating, the COF can be further reduced to 0.02. Friction and wear resistance of both the silicon substrate and the steel ball is significantly enhanced (by one to two orders of magnitude) with such G–TiO$_2$ NS coating. Morphological study of the wear track shows that sharkskin-like hierarchical structures are generated during friction, which is ascribed to the assembly and layering of the G-TiO$_2$ NS. The incommensurate contact area and rolling of G–TiO$_2$ NS during this process are believed to be the major reasons for the achieved outstanding solid lubrication performance. The scalable generation of such hybrid nanoscrolls as high-performance solid lubricants will have impact on aerospace, automotive, and precision manufacturing.

Declarations

References

1. Scharf, T.W., Prasad, S.V.: Solid lubricants: a review. J. Mater. Sci. **48**, 511–531 (2013)
2. Rosenkranz, A., Costa, H.L., Baykara, M.Z., Martini, A.: Synergetic effects of surface texturing and solid lubricants to tailor friction and wear—a review. Tribol. Int. **155**, 106792 (2021)
3. Kumar, R., Banga, H.K., Singh, H., Kundal, S.: An outline on modern day applications of solid lubricants. Mater. Today: Proc. **28**, 1962–1967 (2020)
4. Ayyagari, A.V., Mutyala, K.C., Sumant, A.V.: Towards developing robust solid lubricant operable in multifarious environments. Sci. Rep. **10**(1), 15390 (2020)
5. Vazirisereshk, M.R., Martini, A., Strubbe, D.A., Baykara, M.Z.: Solid lubrication with MoS2: a review. Lubricants **7**(7), 57 (2019)
6. Huai, W., Zhang, C., Wen, S.: Graphite-based solid lubricant for high-temperature lubrication. Friction **9**, 1660–1672 (2021)
7. Wu, S., Tian, S., Menezes, P.L., Xiong, G.: Carbon solid lubricants: role of different dimensions. Int. J. Adv. Manuf. Technol. **107**, 3875–3895 (2020)
8. Donnet, C., Erdemir, A.: Historical developments and new trends in tribological and solid lubricant coatings. Surf. Coat. Technol. **180**, 76–84 (2004)
9. Liang, H., Bu, Y., Zhang, J., Cao, Z., Liang, A.: Graphene oxide film as solid lubricant. ACS Appl. Mater. Interfaces **5**(13), 6369–6375 (2013)
10. Kim, K.S., Lee, H.J., Lee, C., Lee, S.K., Jang, H., Ahn, J.H., Kim, J.H., Lee, H.J.: Chemical vapor deposition-grown graphene: the thinnest solid lubricant. ACS Nano **5**(6), 5107–5114 (2011)
11. Jin, B., Chen, G., He, Y., Zhang, C., Luo, J.: Lubrication properties of graphene under harsh working conditions. Mater. Today Adv. **18**, 100369 (2023)
12. Chowdhury, T., Kim, J., Sadler, E.C., Li, C., Lee, S.W., Jo, K., Xu, W., Gracias, D.H., Drichko, N.V., Jariwala, D., Brintlinger, T.H., Mueller, T., Park, H.G., Kempa, T.J.: Substrate-directed synthesis of MoS2 nanocrystals with tunable dimensionality and optical properties. Nat. Nanotechnol. **15**, 29–34 (2020)
13. Mutyala, K.C., Wu, Y.A., Erdemir, A., Sumant, A.V.: Graphene-MoS2 ensembles to reduce friction and wear in DLC-steel contacts. Carbon **146**, 524–527 (2019)
14. Manu, B.R., Gupta, A., Jayatissa, A.H.: Tribological properties of 2D materials and composites—a review of recent advances. Materials **14**(7), 1630 (2021)
15. Berman, D., Deshmukh, S.A., Sankaranarayanan, S.K., Erdemir, A., Sumant, A.V.: Macroscale superlubricity enabled by graphene nanoscroll formation. Science **348**(6239), 1118–1122 (2015)
16. Gong, Z., Shi, J., Zhang, B., Zhang, J.: Graphene nano scrolls responding to superlow friction of amorphous carbon. Carbon **116**, 310–317 (2017)
17. Zhang, Z., Du, Y., Huang, S., Meng, F., Chen, L., Xie, W., Chang, K., Zhang, C., Lu, Y., Lin, C.T., Li, S., Parkin, I.P., Guo, D.: Macroscale superlubricity enabled by graphene-coated surfaces. Adv. Sci. **7**(4), 1903239 (2020)
18. Zheng, B., Xu, Z., Gao, C.: Mass production of graphene nanoscrolls and their application in high rate performance supercapacitors. Nanoscale **8**(3), 1413–1420 (2016)
19. Xu, Z., Zheng, B., Chen, J., Gao, C.: Highly efficient synthesis of neat graphene nanoscrolls from graphene oxide by well-controlled lyophilization. Chem. Mater. **26**(23), 6811–6818 (2014)
20. Sharifi, T., Gracia-Espino, E., Reza Barzegar, H., Jia, X., Nitze, F., Hu, G., Nordblad, P., Tai, C.W., Wågberg, T.: Formation of nitrogen-doped graphene nanoscrolls by adsorption of magnetic γ-Fe2O3 nanoparticles. Nat. Commun. **4**(1), 2319 (2013)
21. Chen, X., Li, L., Sun, X., Kia, H.G., Peng, H.: A novel synthesis of graphene nanoscrolls with tunable dimension at a large scale. Nanotechnology **23**(5), 055603 (2012)
22. Liu, Y., Mateti, S., Li, C., Liu, X., Glushenkov, A.M., Liu, D., Li, L.H., Fabijanic, D., Chen, Y.: Synthesis of composite nanosheets of graphene and boron nitride and their lubrication application in oil. Adv. Eng. Mater. **20**(2), 1700488 (2018)
23. Tabandeh-Khorshid, M., Omrani, E., Menezes, P.L., Rohatgi, P.K.: Tribological performance of self-lubricating aluminum matrix nanocomposites: role of graphene nanoplatelets. Eng. Sci. Technol. Int. J. **19**(1), 463–469 (2016)
24. Van Sang, Le., Sugimura, N., Khajeh, K., Washizu, H.: Solid lubricants of combined graphene and iron nanoparticles for study of friction and stability. Langmuir **38**(5), 1860–1868 (2022)
25. Guo, P., Chen, L., Wang, J., Geng, Z., Lu, Z., Zhang, G.: Enhanced tribological performance of aminated nano-silica modified graphene oxide as water-based lubricant additive. ACS Appl. Nano Mater. **1**(11), 6444–6453 (2018)
26. Ewen, J.P., Gattinoni, C., Thakkar, F.M., Morgan, N., Spikes, H.A., Dini, D.: Nonequilibrium molecular dynamics investigation

of the reduction in friction and wear by carbon nanoparticles between iron surfaces. Tribol. Lett. **63**, 1–15 (2016)

27. Meng, Y., Su, F., Chen, Y.: Synthesis of nano-Cu/graphene oxide composites by supercritical CO2-assisted deposition as a novel material for reducing friction and wear. Chem. Eng. J. **281**, 11–19 (2015)

28. Liu, S., Kasbe, P.S., Yang, M., Shen, N., Duan, L., Mao, Y., Xu, W.: Intimately bonded 2D materials and responsive polymer brushes for adaptive nanocomposites. Polymer **210**, 123033 (2020)

29. Shimizu, W., Nakamura, S., Sato, T., Murakami, Y.: Creation of high-refractive-index amorphous titanium oxide thin films from low-fractal-dimension polymeric precursors synthesized by a sol-gel technique with a hydrazine monohydrochloride catalyst. Langmuir **28**(33), 12245–12255 (2012)

30. Ma, B., Rodriguez, R.D., Ruban, A., Pavlov, S., Sheremet, E.: The Correlation between electrical conductivity and second-order raman modes of laser-reduced graphene oxide. Phys. Chem. Chem. Phys. **21**(19), 10125–10134 (2019)

31. Chen, C.A., Huang, Y.S., Chung, W.H., Tsai, D.S., Tiong, K.K.: Raman spectroscopy study of the phase transformation on nanocrystalline titania films prepared via metal organic vapour deposition. J. Mater. Sci.: Mater. Electron. **20**, 303–306 (2009)

32. Du, S., Sun, J., Wu, P.: Preparation, characterization and lubrication performances of graphene oxide-TiO2 nanofluid in rolling strips. Carbon **140**, 338–351 (2018)

33. Low, F.W., Chin Hock, G., Kashif, M., Samsudin, N.A., Chau, C.F., Indah Utami, A.R., Aminul Islam, M., Heah, C.Y., Liew, Y.M., Lai, C.W., et al.: Influence of sputtering temperature of TiO2 deposited onto reduced graphene oxide nanosheet as

efficient photoanodes in dye-sensitized solar cells. Molecules **25**(20), 4852 (2020)

34. Xing, M., Shen, F., Qiu, B., Zhang, J.: Highly-dispersed boron-doped graphene nanosheets loaded with TiO2 nanoparticles for enhancing CO2 photoreduction. Sci. Rep. **4**(1), 6341 (2014)

35. Ivan, R., Popescu, C., del Pino, A.P., Yousef, I., Logofatu, C., György, E.: Laser-induced synthesis and photocatalytic properties of hybrid organic-inorganic composite layers. J. Mater. Sci. **54**(5), 3927–3941 (2019)

36. Berman, D., Erdemir, A., Sumant, A.V.: Graphene: a new emerging lubricant. Mater. Today **17**(1), 31–42 (2014)

37. Wang, L.F., Ma, T.B., Hu, Y.Z., Wang, H.: Atomic-scale friction in graphene oxide: an interfacial interaction perspective from first-principles calculations. Phys. Rev. B **86**(12), 125436 (2012)

38. Ilie, F., Ipate, G., Manaila, F.C.: Tribological properties study of solid lubrication with TiO2 powder particles. Materials **15**(20), 7145 (2022)

39. Chen, D., Liu, Y., Chen, H., Zhang, D.: Bio-inspired drag reduction surface from sharkskin. Biosurf. Biotribol. **4**(2), 39–45 (2018)

40. Huang, Q., Shi, X., Xue, Y., Zhang, K., Gao, Y., Wu, C.: Synergetic effects of biomimetic microtexture with multi-solid lubricants to improve tribological properties of AISI 4140 steel. Tribol. Int. **167**, 107395 (2022)

Authors and Affiliations

Pratik S. Kasbe[1] · Juan Bosch[2] · Jinyu Bu[1] · Christopher DellaCorte[2] · Weinan Xu[1]

✉ Christopher DellaCorte
   cdellacorte@uakron.edu

✉ Weinan Xu
   weinanxu@uakron.edu

[1]   School of Polymer Science and Polymer Engineering, The University of Akron, Akron, OH 44325, USA

[2]   Department of Mechanical Engineering, The University of Akron, Akron, OH 44325, USA